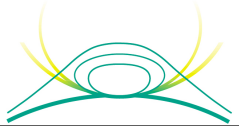

SFB 609

Sonderforschungsbereich 609
Elektromagnetische Strömungsbeeinflussung in
Metallurgie, Kristallzüchtung und Elektrochemie

M. Hinze, S. Ziegenbalg

Optimal control of the free boundary in a two-phase Stefan problem with flow driven by convection

SFB-Preprint SFB609-02-2006

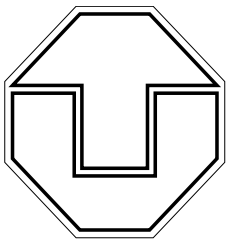

TECHNISCHE
UNIVERSITÄT
DRESDEN

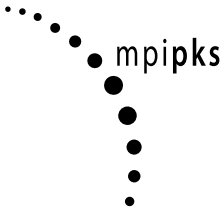

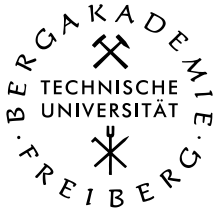

Preprint Reihe
SFB 609

Diese Arbeit ist mit Unterstützung des von der Deutschen Forschungsgemeinschaft getragenen Sonderforschungsbereiches 609 entstanden und als Manuskript vervielfältigt worden.

Dresden, October 2006

The list of preprints of the Sonderforschungsbereich 609 is available at: http://www.tu-dresden.de/sfb609/pub.html

Abstract

We present an optimal control approach for the solidification process of a melt in a container. The process is described by a two phase Stefan problem including flow driven by convection and Lorentz forces. The free boundary (interface between the two phases) is modelled as a graph.

We control the evolution of the free boundary using the temperature on the container wall and/or the Lorentz forces. The control goal consists in tracking a prescribed evolution of the free boundary. We achieve this goal by minimizing a appropriate cost functional. The resulting minimization problem is solved numerically by a steepest descent method with step size control, where the gradient of the cost functional is expressed in terms of the adjoint variables. Several numerical examples are presented which illustrate the performance of the method.

1 Introduction

In the present work we extend our control approach to solidification processes presented in [3]. Here we also include flow driven by convection and in addition to temperature boundary control we also consider near wall Lorentz forces as control actions. We develop an optimization strategy for the free boundary in the corresponding two phase Stefan problem, whose mathematical model in the present situation governs heat conduction in the solid phase and heat conduction, heat transport and flow in the liquid phase. The coupling of the phases is established through the Stefan condition at the free boundary, and through a third order boundary condition which follows from the heat transfer equation at the container wall.

Our goal is to control the evolution of the free boundary using the temperature at the container wall and/or near-wall Lorentz forces as control action. This is motivated by the fact, that we have in mind control of crystal growth processes, where the shape of the solid-liquid interface strongly influences the quality of the crystal.

We assume that the free boundary can be described by a graph. This leads to a sharp interface model which explicitly contains the free boundary control variable in terms of the function which defines its graph. The mathematical formulation of the control goal now reads: for a prescribed desired evolution described as a graph, find a temperature boundary control and/or near-wall Lorentz forces such that the free boundary of the system is as close as possible to the desired free boundary. Since the free boundary is modelled as a graph, its error to the desired free boundary can be formulated in form of a cost

functional which explicitly contains the described functions.

Altogether we end up with an optimization problem for the temperature on the container wall and/or near-wall Lorentz forces, which is coupled to the temperature in the solid and liquid phases, to the velocity in the liquid phase and to the desired free boundary by an highly nonlinear system of pde's.

Let us comment on the work of Zabaras et al. In [7], [10], [9] similar control problems as in the present work are considered. The main differences to our have their origin in the fact that the free boundary is assumed as known a priori and that the melting temperature condition at the free boundary is not met exactly during the optimization process. This may lead to unphysical solutions of the control approach. This is in contrast to our approach, where at any stage of the optimization procedure developed the physical laws constituted by our model are conserved.

In [7] and [10] the free boundary is set to the desired boundary without ensuring that the melting temperature condition $u = u_m$ is satisfied at the free boundary (u denotes the temperature, u_m denotes the melting temperature). The heat flow at the fixed boundary into the liquid phase is set to 0 (this means, that the container is isolated). This allows to separate the problems for each phase. In particular, the heat flow into the free boundary can be computed using the Stefan condition, and by solving a direct (forward) heat conduction problem [7], or a direct (forward) heat conduction problem including convection [10]. The optimization goal consists in determining the heat flux at the fixed boundary of the solid phase such that the temperature difference at the free boundary is minimized, i.e. $\frac{1}{2}\|u_m - u(x,t)\|^2_{L_2(\Gamma\times[0,T])} = \min_{q_0}$, where q_0 is the heat flow into the solid phase at the fixed boundary.

Yang in [9] extends the approach of [10] to the case where the temperature at the fixed boundary in the liquid phase is also variable. To separate the problems for each phase the heat flux into the free boundary is assumed to be given. The minimization problem in the liquid phase consists in determining the temperature at the fixed boundary considering heat conduction, convection and the Stefan condition, such that the error of the temperature at the free boundary $\|u_m - u(x,t)\|^2_{L_2(\Gamma\times[0,T])}$ is minimized, with the position of the free boundary and heat flux into the free boundary given. The minimization problem for the solid phase then reads as in [7] and [10]: Given the position and the heat flux of the free boundary, find the heat flux on the fixed boundary such that the error of the temperature at the free boundary is minimized.

The approaches of Zabaras at al. and Yang have in common, that a physical solution of the optimization process is obtained only in the case $\|u_m - u(x,t)\|^2_{L_2(\Gamma\times[0,T])} = 0$, which in most configurations only is satisfied by chance. We emphasize that the approach presented here always delivers

physical solutions.

For a discussion on further related literature we refer to [3]. To the best of our knowledge this is the first attempt (except of our previous work [3]) to control the evolution of the free boundary directly using a sharp interface model. The presented approach admits the major advantage, that the interface serves as an optimization variable itself and thus can be controlled directly. This is different to phase field models, say, where the free boundary is represented as a zero level set which only admits indirect control through the order parameter. Furthermore at any stage of the optimization process the physical laws constituted by our mathematical model are conserved.

2 Problem definition

2.1 Physical model

Let $\Omega = G \times H$ be a bounded cylindrical domain containing the substance, where G denotes the ground domain and $H \subset \mathbb{R}$ the height, see Figure 1. For $t \in [0,T]$ let $\Omega_s(t), \Omega_l(t) \subset \Omega$ denote the parts containing the solid and the liquid phase, where $\Omega_s(t) \cap \Omega_l(t) = \emptyset$ and $\overline{\Omega} = \overline{\Omega_s(t)} \cup \overline{\Omega_l(t)}$. The free boundary is described as a graph

$$\Gamma(t) := \overline{\Omega_s(t)} \cap \overline{\Omega_l(t)} = \left\{ \begin{pmatrix} y \\ f(t,y) \end{pmatrix} : y \in G \right\}$$

with $f : G \to H$. Figure 1 shows such a configuration.

As mathematical model for the temperature u, the velocity $\boldsymbol{v}$ and the pressure p we take

$$\partial_t u = \frac{k_s}{c_s \rho} \Delta u \qquad \text{in } (0,T] \times \Omega_s \quad (1)$$

$$\partial_t u + \boldsymbol{v} \cdot \nabla u = \frac{k_l}{c_l \rho} \Delta u \qquad \text{in } (0,T] \times \Omega_l \quad (2)$$

$$\nabla \cdot \boldsymbol{v} = 0 \qquad \text{in } (0,T] \times \Omega_l \quad (3)$$

$$\partial_t \boldsymbol{v} + (\nabla \boldsymbol{v})\boldsymbol{v} - \frac{\varepsilon}{\rho} \Delta \boldsymbol{v} + \frac{1}{\rho} \nabla p = -\boldsymbol{g} \gamma (u - u_M) + \boldsymbol{A} \qquad \text{in } (0,T] \times \Omega_l \quad (4)$$

$$V_\Gamma L = \frac{k_s}{\rho} \partial_{\boldsymbol{\mu}} u|_{\Omega_s} - \frac{k_l}{\rho} \partial_{\boldsymbol{\mu}} u|_{\Omega_l} =: -\left[\frac{k_{s/l}}{\rho} \partial_{\boldsymbol{\mu}} u \right]_\Gamma \qquad \text{on } (0,T] \times \Gamma \quad (5)$$

$$u = u_M \qquad \text{on } (0,T] \times \Gamma \quad (6)$$

with the initial conditions

$$u(0, \boldsymbol{x}) = u_0(x) \qquad \text{for } \boldsymbol{x} \in \Omega \tag{7}$$
$$\boldsymbol{v}(0, \boldsymbol{x}) = \boldsymbol{v}_0(x) \qquad \text{for } \boldsymbol{x} \in \Omega \tag{8}$$
$$f(0, y) = f_0(y) \qquad \text{for } y \in G \tag{9}$$

and the boundary conditions

$$\tfrac{k_{s/l}}{\alpha_{s/l}} \partial_{\boldsymbol{\nu}} u = u_b - u \qquad \text{on } (0, T] \times \partial\Omega \tag{10}$$
$$\boldsymbol{v} = 0 \qquad \text{on } (0, T] \times \partial\Omega \tag{11}$$
$$\partial_{\boldsymbol{\nu}} p = -\rho \boldsymbol{\nu} \cdot \boldsymbol{g} \gamma (u - u_M) + \boldsymbol{\nu} \cdot \boldsymbol{A} \qquad \text{on } (0, T] \times \partial\Omega_l. \tag{12}$$

The vector $\boldsymbol{\nu}$ denotes the outer normal vector of the boundary and $\boldsymbol{\mu}$ denotes the normal vector of the free boundary, directed from the solid into the liquid phase (i.e. $\boldsymbol{\mu} = \boldsymbol{\nu}|_{\partial\Omega_s} = -\boldsymbol{\nu}|_{\partial\Omega_l}$ on Γ). Equations (3) and (4) form the Navier Stokes equations for incompressible flow, where ε denotes the dynamic viscosity and ρ denotes the density. The buoyancy force is modelled with the Boussinesq approximation by the term $-\boldsymbol{g}\gamma(u - u_M)$ using the gravitational force $\boldsymbol{g}$ and the thermal expansion coefficient γ. The external force $\boldsymbol{A}$ is used later in this section to model the Lorentz force. Equations (1) and (2) are the heat equation in the solid phase and the heat equation with heat transport in the liquid phase, respectively. The constants $k_{s/l}$ and $c_{s/l}$ denotes the heat conductivities and the heat capacity in the solid and liquid phase, respectively. The Stefan condition (5) is a conservation law on the free boundary which balances the heat transported into the free boundary and the melting heat generated through solidification. The constant L denotes the latent heat.

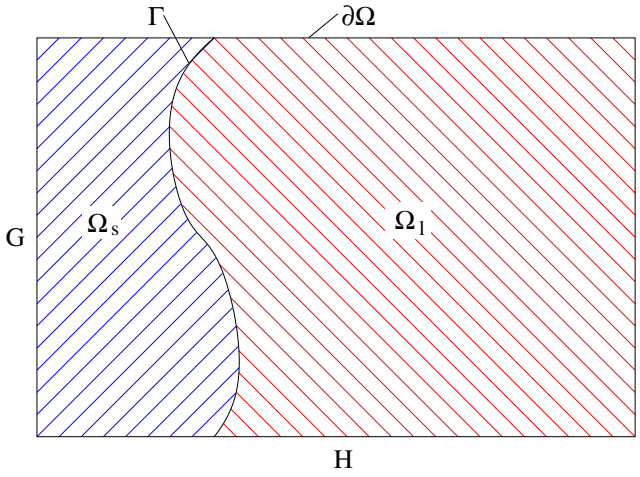

Figure 1: Solid phase Ω_s, liquid phase Ω_l and free boundary Γ in a container with boundary $\partial\Omega$.

Using the free boundary graph f the Stefan condition (5) can be equivalently written as

$$L\rho \frac{f_t(t,y)}{\sqrt{1+f_y(t,\boldsymbol{x})}} = -\left[k_{s/l}\partial_{\boldsymbol{\mu}} u\right]_\Gamma \left(t, \begin{pmatrix} y \\ f(t,y) \end{pmatrix}\right) = 0 \ .$$

Equation (6) states the melting temperature condition, where u_M is the melting temperature. The boundary condition (10) for the temperature follows directly from the heat transfer equation $q = \alpha_{s/l}(u - u_b)$ and the heat conduction $q = k_{s/l}\partial_\nu u$, where q is the heat flow and $\alpha_{s/l}$ is the heat transfer coefficient between the container wall and the solid/liquid phase, respectively.

For the modeling of the Lorentz forces we consider a (hypothetical) rotational symmetric configuration with $G = \big\{(r\cos\phi, r\sin\phi) : \phi \in [0, 2\pi], r \in [0, R]\big\}$ and $h \in H = [h_a, h_b]$ as sketched in Figure 2. This configuration consists of actuator rings of the thickness $dh \to 0$. Each ring consists of an alternating arrangement of electrodes and magnets and each ring is controllable separately. We assume that the Lorentz force of each ring is rotational symmetric and acts only in tangential direction, see Figure 3. This allows us to assemble the total Lorentz force at $\boldsymbol{x} = (r\cos\phi, r\sin\phi, h)$ by integration over the Lorentz forces generated by each ring

$$\boldsymbol{A}(\boldsymbol{x}) = \delta \int_H A_c(y)\boldsymbol{\tau}(x,y) g\big(\sqrt{(R-r)^2 + (h-y)^2}\big) dy \tag{13}$$

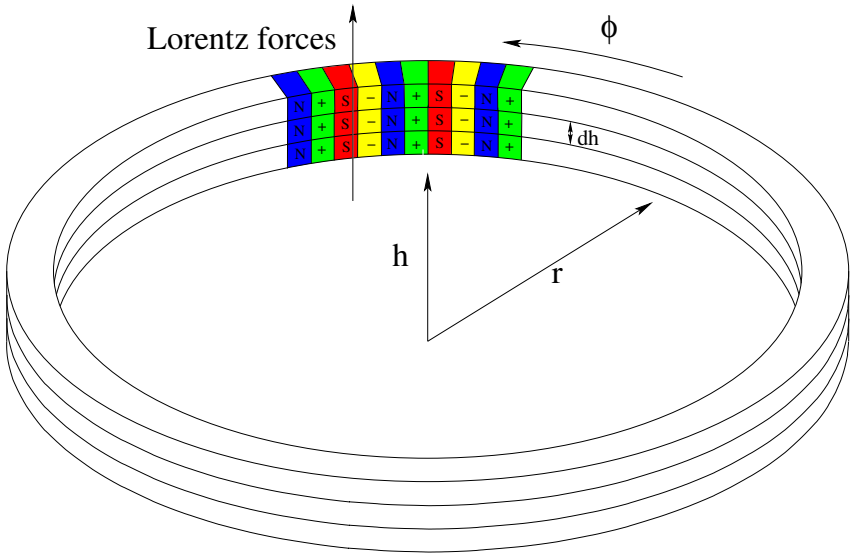

Figure 2: Configuration of actuator rings used for generating Lorentz forces.

where

$$\boldsymbol{\tau} = \frac{\big((h-y)\cos\phi, (h-y)\sin\phi, (R-r)\big)}{\sqrt{(R-r)^2+(h-y)^2}} \ , \tag{14}$$

is the tangential vector (see Figure 3) and A_c is the control force. The constant δ is used to tailor the influence of the control force. The function $g(r)$ denotes the dependency of the Lorentz force from the distance d, see Figure 3. We choose

$$g(d) = \frac{e^{-d\frac{\pi}{a}}}{2\sqrt{d}} \ .$$

With this choice for g and $A_c = \text{const.}$ we obtain wall-parallel Lorentz forces in h-direction which satisfy the approximation

$$A(\boldsymbol{x}) \approx \delta A_c e^{-\frac{\pi}{a}\,\mathrm{dist}(\boldsymbol{x},\partial G\times H)} \ ,$$

compare [2, Appendix] and [8, Section 2,4]. Here a denotes the width of the electrodes and magnets. We note, that we ignore effects caused by induction. This makes sense for weakly conductive fluids and partially also for high conductive fluids, if we use small magnetic and strong electric fields. Let us note that highly conductive fluids combined with strong electric fields would cause a considerable heating of the material near the container wall, which is not considered in our model.

Let $\overline{f}$ be the desired evolution of the free boundary. We consider the rotational symmetric case, i.e. $G = \big\{(r\cos\phi, r\sin\phi) : \phi \in [0,2\pi], r \in [0,R]\big\}$ and $h \in H = [h_a, h_b]$. Similar to [3], we specify additional boundary conditions for the intersection of the free boundary and the container wall;

$$f(t,R) = \overline{f}(t,R) \qquad f_r(t,R) = \overline{f}_r(t,R) \qquad f_{rr}(t,R) = \overline{f}_{rr}(t,R) \ . \tag{15}$$

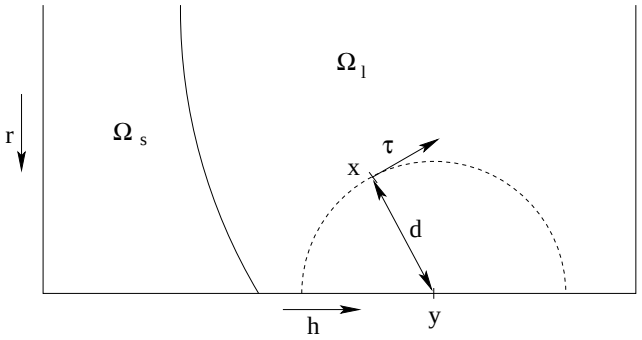

Figure 3: Lorentz forces generated by a single actuator ring.

This choice simplifies our moving grid implementation and especially it avoids the need of an additional boundary grid for the container wall temperature u_b, and so the interpolation of u_b between grids is avoided. further details are given in [3].

The boundary conditions (15) induce the following compatibility conditions;

$$L\rho\frac{\overline{f}_t\overline{f}_r}{1+\overline{f}_r^2} = -(\alpha_s-\alpha_l)u_b \tag{16}$$

$$\begin{aligned}\partial_h u_b\big|_{\Omega_{s/l}} =& \frac{\overline{f}_t}{1+\overline{f}_r^2}\left(\frac{L\rho}{\alpha_s-\alpha_l}\left(\frac{\alpha_{s/l}}{k_{s/l}} - 2\frac{\overline{f}_r\overline{f}_{rr}}{\left(1+\overline{f}_r^2\right)^2}\right) - \frac{u_b\rho c_{s/l}}{k_{s/l}}\right)\\ &+ \frac{L\rho\overline{f}_{rt}}{(\alpha_s-\alpha_l)\left(1+\overline{f}_r^2\right)^2}\ .\end{aligned} \tag{17}$$

For the two-dimensional case the boundary conditions for f and the corresponding compatibility conditions are presented in [3], where also a detailed derivation of the compatibility condition is given. We note, the flow has no influence on the derivation since $\boldsymbol{v}$ satisfies $\boldsymbol{v}=0$ at the boundary $\partial\Omega_l$.

Further we need to ensure that the boundary conditions are satisfied for $t=0$, i.e. we to set

$$u_b(0,\boldsymbol{x}) = u_0(\boldsymbol{x}) + \tfrac{k_{s/l}}{\alpha_{s/l}}\partial_\nu u_0(\boldsymbol{x})\ . \tag{18}$$

Since u_b needs to satisfy the compatibility conditions (16) – (18) it cannot serve as control variable directly. We resolve this difficulty by splitting u_b into two parts;

$$u_b = u_{b0} + \beta u_{bc} \tag{19}$$

where u_{b0} denotes a fixed part (e.g. a temperature known from experience), and βu_{bc} denotes the controllable part βu_{bc}, where β is a weight function which allows to tailor the control part of the boundary condition. Now we require that u_{b0} satisfies the compatibility conditions (16) – (18) and assume

$$\begin{aligned}&\beta(t,\boldsymbol{x}) = \partial_{e_2}\beta(t,\boldsymbol{x}) = 0 \qquad && \text{for } \boldsymbol{x}\in\partial\Omega\cap\Gamma \text{ and } t\in(0,T],\\ &\beta(0,\boldsymbol{x}) = 0 && \text{for } \boldsymbol{x}\in\partial\Omega.\end{aligned} \tag{20}$$

These conditions ensure that u_b for every choice u_{bc} satisfies (16) – (18), so that u_{bc} may serve as the control variable in our optimization problem specified below.

2.2 Optimization Problem

Our goal is to control the free boundary using the temperature on the container walls and/or near-wall Lorentz forces. As control horizon we take $t \in (0, T]$ for some $T > 0$. Using the desired evolution of the free boundary $\overline{f}$ we define the optimization problem

$$\begin{aligned} J(f, u_{bc}, \boldsymbol{A}_c) :=& \frac{1}{2T} \int_0^T \int_G \big(f(t,y) - \overline{f}(t,y)\big)^2 dy dt \\ &+ \frac{\lambda_T}{2} \int_G \big(f(T,y) - \overline{f}(T,y)\big)^2 dy = \min_{f, u_{bc}, \boldsymbol{A}_c}! \\ \text{s.t. } (1) - (12), (13), (19) \quad & . \end{aligned} \tag{21}$$

The functional J models the objective in our minimization problem, namely the reduction of the error between the free boundary and the desired free boundary. With λ_T the deviation of the free boundary from the desired free boundary at time $t = T$ is weighed. The functions u_{b0}, β, $\overline{f}$, u_0, f_0 and $\boldsymbol{v}_0$ are given and the functions u, f, $\boldsymbol{v}$ and u_{bc} and/or A_c are sought. From here onwards we assume that the optimization problem admits a solution $(u^*, f^*, \boldsymbol{v}^*, u_{bc}^*, A_c^*)$. Further we assume that the state equations (1) – (12), (13), (19) for every (u_{bc}, A_c) admit a unique solution, in particular $f = f(u_{bc}, A_c)$. It then is meaningful to replace (21) by

$$K(u_{bc}, \boldsymbol{A}_c) := J\big(f(u_{bc}, \boldsymbol{A}_c), u_{bc}, \boldsymbol{A}_c\big) = \min_{u_{bc}, \boldsymbol{A}_c}! \ , \tag{22}$$

where k denotes the reduced functional. To solve this optimization problem numerically in Section 3 we apply a gradient algorithm with a appropriate step size rule. Thus we need an expression for $\nabla K(u_{bc}, \boldsymbol{A}_c)$. There holds

$$\nabla K = \Big[-\beta \alpha_{s/l} \omega_{s/l} \ , \quad -\delta \int_{\Omega_l} \boldsymbol{\psi}(t, \boldsymbol{x}) \cdot \boldsymbol{\tau}(\boldsymbol{x}, y) g\big(\sqrt{(R-r)^2 + (h-y)^2}\big) d\boldsymbol{x} \Big] \tag{23}$$

where $\boldsymbol{x} = (r\cos\phi, r\sin\phi, h)$ and the tangential vector $\boldsymbol{\tau}$ is defined as in (14), see also Figure 3. For given u_{bc} and A_c the functions $\omega_{s/l}$ and $\boldsymbol{\psi}$ are obtained first by solving (1) – (12), (13), (19) for u, $\boldsymbol{v}$ and f, and then by solving the

so called adjoint system

$$
\begin{aligned}
-\partial_t \omega_s &= \frac{k_s}{c_s \rho} \Delta \omega_s && \text{in } [0,T) \times \Omega_s \ , && (24)\\
-\partial_t \omega_l &= \frac{k_l}{c_l \rho} \Delta \omega_l + \boldsymbol{v} \cdot \nabla \omega_l - \frac{\gamma \boldsymbol{g}}{c_l \rho} \cdot \boldsymbol{\psi} && \text{in } [0,T) \times \Omega_l \ , && (25)\\
k_{s/l} \partial_{\boldsymbol{\nu}} \omega_{s/l} &= -\alpha_{s/l} \omega_{s/l} && \text{in } [0,T) \times \partial\Omega_{s/l} \setminus \Gamma \ , && (26)\\
\omega_{s/l} &= 0 && \text{in } \{T\} \times \Omega_{s/l} \ , && (27)\\
\omega_{s/l} &= -\varphi && \text{in } (0,T) \times \Gamma \ , && (28)
\end{aligned}
$$

$$
\begin{aligned}
\partial_t \boldsymbol{\psi} + (\nabla \boldsymbol{\psi}) \boldsymbol{v} - (\nabla \boldsymbol{v})^T \boldsymbol{\psi} + \frac{\varepsilon}{\rho} \Delta \boldsymbol{\psi} &= c_l \rho \omega_l \nabla u - \nabla \pi && \text{in } [0,T) \times \Omega_l \ , && (29)\\
\boldsymbol{\psi}(T, \boldsymbol{x}) &= 0 && \text{in } \{T\} \times \Omega_l(t) \ , && (30)\\
\boldsymbol{\psi} &= 0 && \text{in } [0,T) \times \partial\Omega_l \ , && (31)\\
\partial_{\boldsymbol{\nu}} \pi &= \partial_{\boldsymbol{\nu}} u c_l \rho \omega_l && \text{in } [0,T) \times \partial\Omega_l \ , && (32)\\
\nabla \cdot \boldsymbol{\psi} &= 0 && \text{in } [0,T) \times \Omega_l \ , && (33)\\
-L\rho \partial_t \varphi &= \frac{\overline{f} - f}{T} && \text{in } [0,T) \times G \ , && (34)\\
L\rho\varphi &= \lambda_T \big(\overline{f} - f\big) && \text{in } \{T\} \times G \text{ and} && (35)\\
\varphi &= 0 && \text{in } (0,T) \times \partial G && (36)
\end{aligned}
$$

for ω, $\boldsymbol{\psi}$ and φ.

3 The numerical approach

In this section we present a numerical solution of the optimization problem

$$K(u_{bc}, \boldsymbol{A}_c) = \min_{u_{bc}, \boldsymbol{A}_c}! \ ,$$

using the following gradient algorithm.

(C0) Initialization of $u_{bc}^{(0)} = 0$ and $\boldsymbol{A}_c^{(0)} = \boldsymbol{0}$
(FWD) Solving the forward system $[u^{(0)}, \boldsymbol{v}^{(0)}, f^{(0)}](u_{bc}^{(0)}, \boldsymbol{A}_c^{(0)})$
(S1) For all $1 \leq k \leq k_{\max}$
(ADJ) Solving of the adjoint equation system $[\omega^{(k)}, \boldsymbol{\psi}^{(k)}, \varphi^{(k)}](u^{(k-1)}, \boldsymbol{v}^{(k-1)}, f^{(k-1)})$
(GRD) Computation of the gradient $G^{(k)} = \nabla K(\omega^{(k)}, \boldsymbol{\psi}^{(k)})$
(LM) Line minimization: $K\big([u_{bc}^{(k-1)}, A_c^{(k-1)}] + s^{(k)} G^{(k)}\big) = \min_{s^{(k)}}!$
(FWD) Solving the forward system $[u^{(k)}, \boldsymbol{v}^{(k)}, f^{(k)}](u_{bc}^{(k)}, \boldsymbol{A}_c^{(k)})$ using $[u_{bc}^{(k)}, A_c^{(k)}] = [u_{bc}^{(k-1)}, A_c^{(k-1)}] + s^{(k)} G^{(k)}$.

The forward and adjoint systems (steps (FWD) and (ADJ)) are discretized using the finite volume approach and are solved using a PISO algorithm, see [4], [5] and [6]. For the spatial discretization we use a moving grid which tracks the free boundary, i.e. the free boundary is represented by a grid hyperplane. A detailed description of this grid can be found in [3]. An example grid for two time instances is shown in Figure 5. For the time discretization we use an adaptive grid where the time steps are calculated by fixing the Courant number. The gradient steps (GRD) are computed according to (23). For the line minimization we use a quadratic approximation approach, which is described in [3]. As stopping criterions we use

$$k_{\max} := \min\left\{k : \frac{J^{(k-1)} - J^{(k)}}{J^{(0)}} \leq \varepsilon\right\} . \tag{37}$$

The algorithm is implemented using the Open Source toolbox OpenFOAM [1].

4 Numerical results

4.1 First test configuration

As the first test problem we consider an aluminium melt in a rotational symmetric cylinder with a diameter of $5cm$ and a height of $10cm$. Thus the domain is described by $\Omega = G \times H$ with the ground $G = \big\{(r\cos\phi, r\sin\phi) : \phi \in [0, 2\pi], r \in [0, R]\big\}$ with $R = 2.5cm$, and the height $H = [h_a, h_b] = [0, 10cm]$. The solid phase is on the bottom and the liquid phase is on the top. The gravitational force is directed downwards, i.e. $\boldsymbol{g} = \big((0,0), -9.82\big)\frac{m}{s^2}$. We optimize the solidification process over the time period $[0, T]$ with $T = 40s$. The physical constants for aluminium are listed in Table 2. For $\alpha_{s/l}$ we choose

$$\alpha_s = 1000\frac{J}{s \cdot cm^2 \cdot K} \qquad \text{and} \qquad \alpha_l = 250\frac{J}{s \cdot cm^2 \cdot K} \ .$$

The desired free boundary is the moving plane $\overline{f}(t, y) = 0.025m + \frac{1}{800}\frac{m}{s} \cdot t$ ($t \in [0, T]$, $y \in G$). As initial condition for the temperature we choose

$$u_0(y, h) = u_M + u'_{s/l}(h - 0.025m) \qquad \text{for } y \in G \text{ and } h \in H,$$

where u'_s and u'_l are equal to

$$u'_{s/l} := \frac{L\rho\alpha_{s/l}}{k_{s/l}(\alpha_s - \alpha_l)} \cdot \frac{1}{800} \cdot \frac{m}{s} \ .$$

For the boundary value u_{b0} we choose

$$u_{b0}\big(t, (y, h)\big) = u_M + u'_{s/l}\big(h - \overline{f}(t, y)\big) \qquad \text{for } t \in [0, T],\ y \in \partial G \text{ and } h \in H.$$

For this choice of $\overline{f}$ the function u_{b0} in (41) satisfies the compatibility conditions (16) – (18).

Two control cases are considered. First, we use only the the container wall temperature u_b for control by setting the control weights β and δ to

$$\beta_1\big(t, (y, h)\big) = \begin{cases} \big(\frac{t}{T}\big)^{0.3} \left(\frac{\overline{f}(t,y) - h}{\overline{f}(t,y)}\right)^2 & : h < \overline{f}(t, y) \\ \big(\frac{t}{T}\big)^{0.3} \left(\frac{h - \overline{f}(t,y)}{h_b - \overline{f}(t,y)}\right)^2 & : h \geq \overline{f}(t, y) \text{ and} \end{cases}$$

$$\delta_1 = 0$$

for $t \in [0, T]$, $y \in \partial G$ and $h \in H$. Secondly, we control using near-wall Lorentz forces only;

$$\beta_2 = 0 \qquad \text{and} \qquad \delta_2 = 1 \ .$$

Making use of the symmetry the spatial mesh contains 100 cells in vertical and 25 cells in radial direction.

The computational time for one forward step (FWD) takes approximately 80s on a single AMD Athlon MP 2133 MHz, for the backward step (ADJ) it takes around 120s.

$\rho = 2650 \frac{kg}{m^3}$	
$c_s = 1230 \frac{J}{kg \cdot K}$	$c_l = 1090 \frac{J}{kg \cdot K}$
$k_s = 227 \frac{J}{s \cdot m \cdot K}$	$k_l = 100 \frac{J}{s \cdot m \cdot K}$
$L = 397670 \frac{J}{kg}$	
$\gamma = 3.84 \cdot 10^{-5} \frac{1}{K}$	
$\varepsilon = 3.23 \cdot 10^{-3} \frac{kg}{m \cdot s}$	
$u_M = 660°\mathrm{C}$	

Table 2: Physical constants aluminium.

4.2 Results for the uncontrolled case

First we examine the results for the uncontrolled forward problem with $u_{bc} = 0$ (Forward step 0 of the algorithm). Figure 4 shows the shape of the free boundary, the temperature u and the velocity v in the liquid phase at three different time instances. Figure 5 shows the corresponding grids.

The images (e.g. in Figure 4) show white and grey stripes. Every stripe represents a temperature interval corresponding to the legend shown right. The black line depicts the free boundary. The arrows are directed into the direction of the flow and their length is proportional to the magnitude of the velocity.

4.3 Results for the controlled case

Fist we examine the control with the container wall temperature, i.e. $\beta = \beta_1$ and $\delta = 0$. We begin our numerical investigation with the setting $\lambda_T = 0$. This means that the error of the free boundary at time T is not penalized.

Figure 6 shows the shape of the free boundary, the temperature and the velocity at two different time instances and after different gradient iterations and when the stopping criterion (37) is met ($k = k_{\max}$). (The plots for $t = 0$

are omitted, since the temperature and the free boundary for all k are equal to the temperature and free boundary, respectively of the uncontrolled problem.) Figure 7 presents the cost functional J for every gradient iteration k. As can be seen the functional

$$J_0 := \frac{1}{2T} \int_0^T \int_G \big(f(t,y) - \overline{f}(t,y)\big)^2 dydt \tag{38}$$

is reduced very quickly, and that the optimized evolution of the free boundary delivers a nearly flat graph at all time instances.

Next, we set $\lambda_T = 0.3$, $\beta = \beta_1$ and $\delta = 0$. The numerical results are presented in Figure 8 (cost Functional) and Figure 9 (temperature, velocity and free boundary). With this parameter choice

$$J_T := \frac{1}{2} \int_G \big(f(T,y) - \overline{f}(T,y)\big)^2 dy \tag{39}$$

is penalized. As expected, our numerical algorithm quickly reduces this functional, see Figure 15, where the behaviour of this part of the functional is

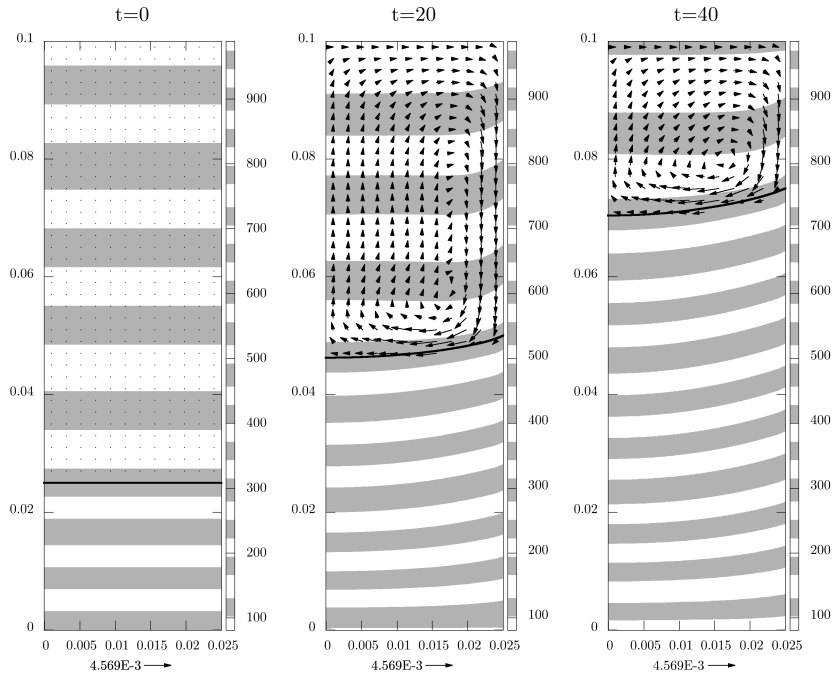

Figure 4: The temperature u (white and grey stripes), the velocity (arrows) and the free boundary (black line) for the uncontrolled problem after three time instances.

illustrated also for different parameter settings. The behaviour of J_0 for the same parameter settings is shown in Figure 14. Again, the graph of the optimized evolution is nearly flat.

Now we investigate the control with near-wall Lorentz forces, i.e. we set $\beta = 0$, $\delta = 1$ and $\lambda_T = 0.3$. The numerical results are presented in Figure 10 (temperature, velocity and free boundary), 11 (Lorentz forces) and 12 (cost Functional). It can be seen, that the control with Lorentz forces does not work as well as with container wall temperature (compare Figure 9). This can be explained using Figure 13. The area around the intersection of the free boundary with the container wall is the coldest zone in the liquid phase. To make the free boundary flat the material of this zone must be transported to the center (dashed arrow). Therefore the Lorentz forces should act in the direction sketched in Figure 13, compare also Figure 11. But the flow driven by that Lorentz forces (and also by the convection) has only a small effect since the velocity is limited due to $\boldsymbol{v} = 0$ at $\partial\Omega_l$ and $\varepsilon > 0$, so that the cold material arrives at the center delayed, i.e. the free boundary is ,,hanging back". (If the Lorentz forces would act in the opposite direction as sketched in Figure 13 the material would be heated up at the container wall and hot material (instead of cold material) would flow to the center.)

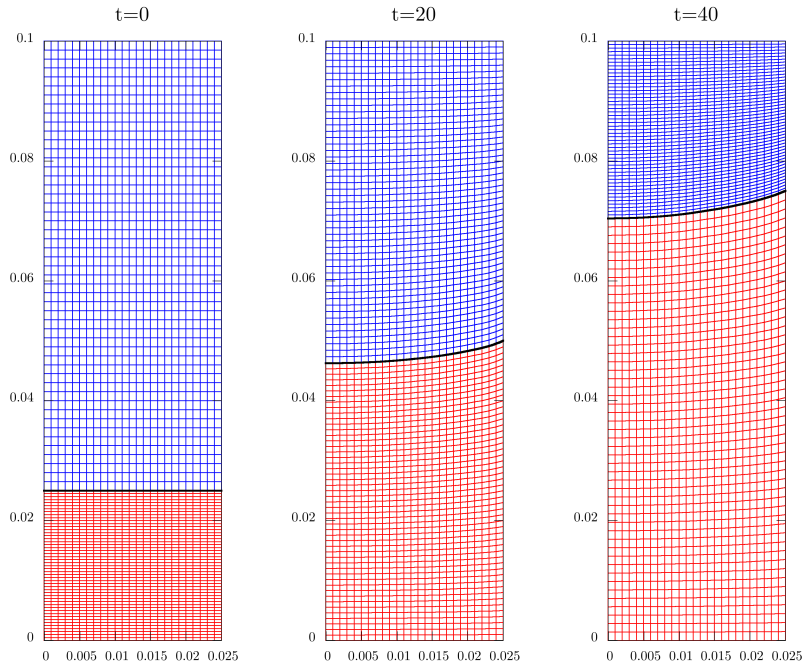

Figure 5: The grid for the uncontrolled problem at three different time instances, see Figure 4. The black line represents the free boundary.

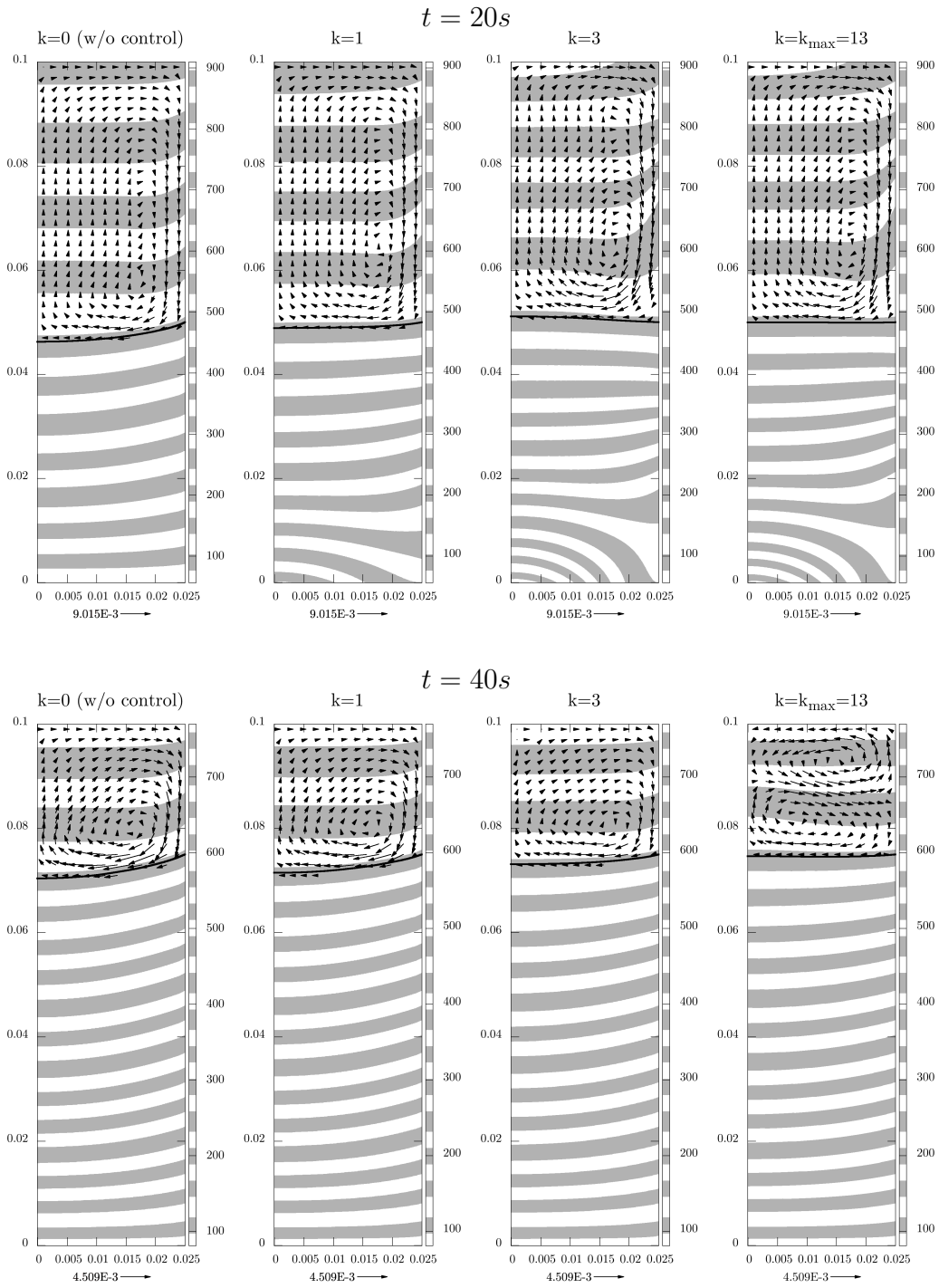

Figure 6: The temperature u (white and grey stripes), velocity (arrows) and free boundary (black line) after several gradient iterations k and at two time instances for the problem with container wall temperature control with $\lambda_T = 0$.

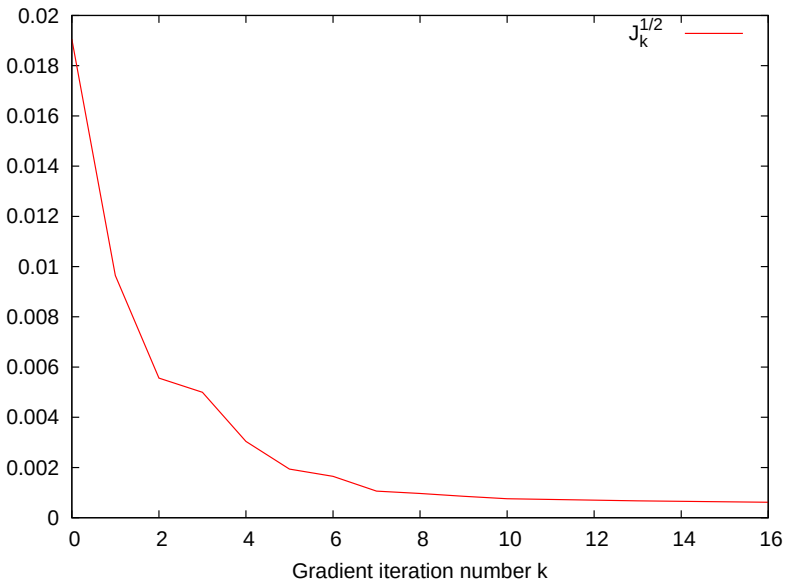

Figure 7: Iteration history of $\sqrt{J}$ for the controlled problem with $\lambda_T = 0$ for each gradient step k for the problem with container wall temperature control.

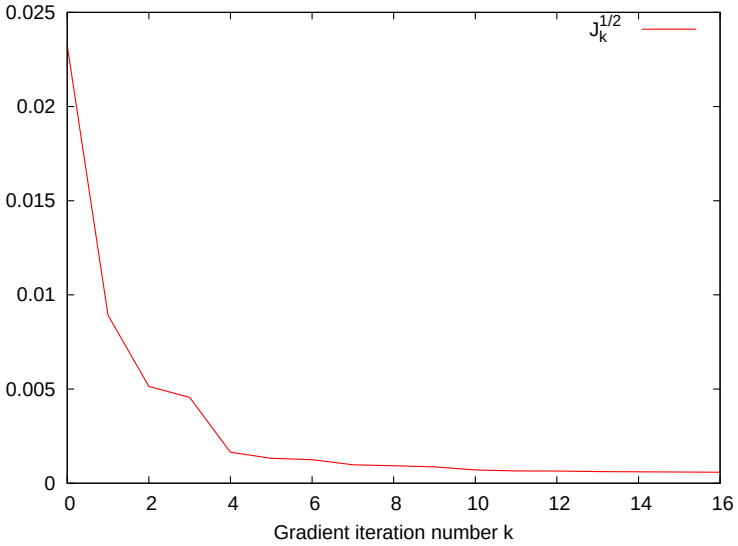

Figure 8: Iteration history of $\sqrt{J}$ for the controlled problem with $\lambda_T = 0.3$ for each gradient step k for the problem with container wall temperature control.

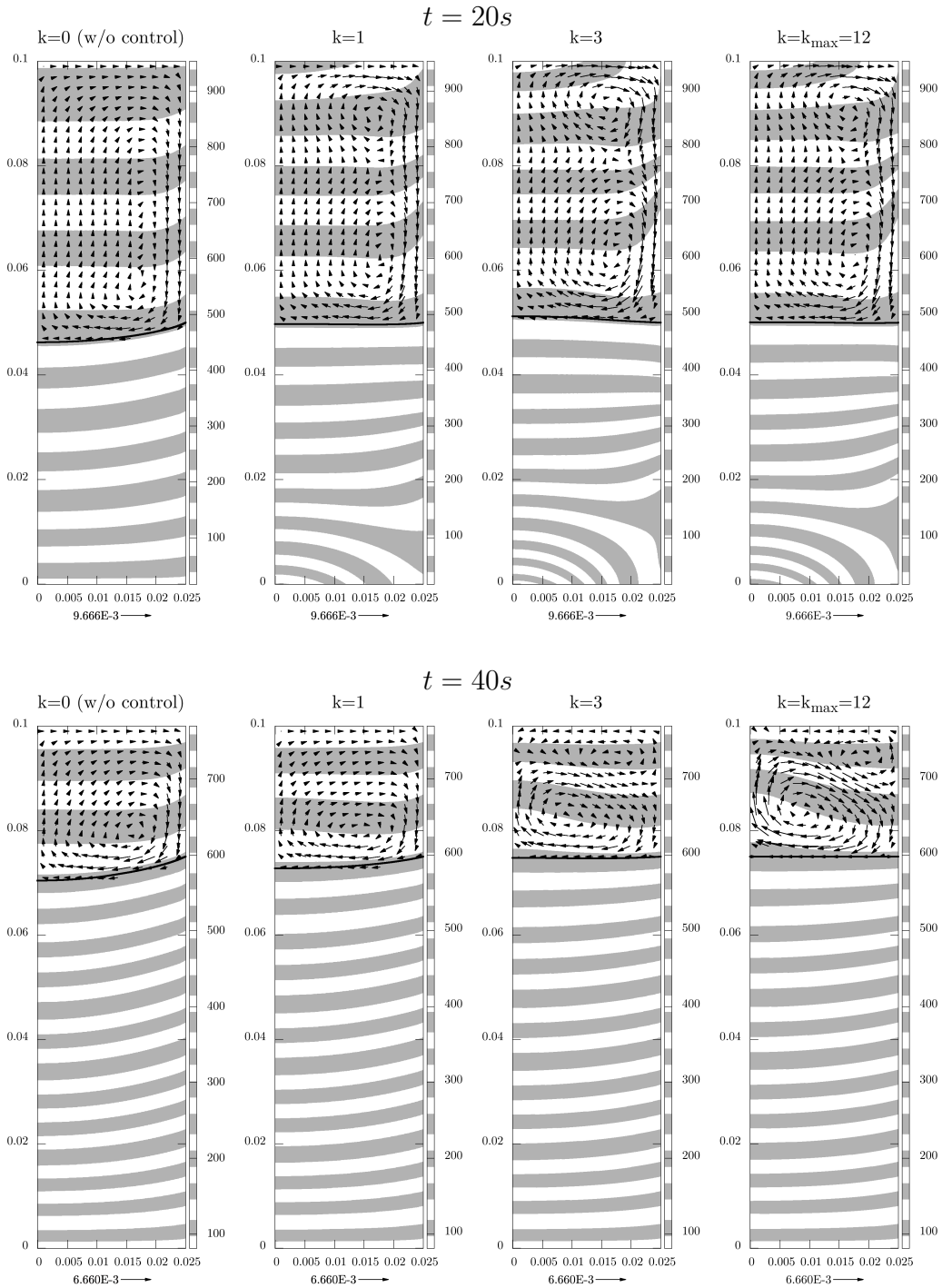

Figure 9: The temperature u (white and grey stripes), velocity (arrows) and free boundary (black line) after several gradient iterations k and at two time instances for the problem with container wall temperature control with $\lambda_T = 0.3$.

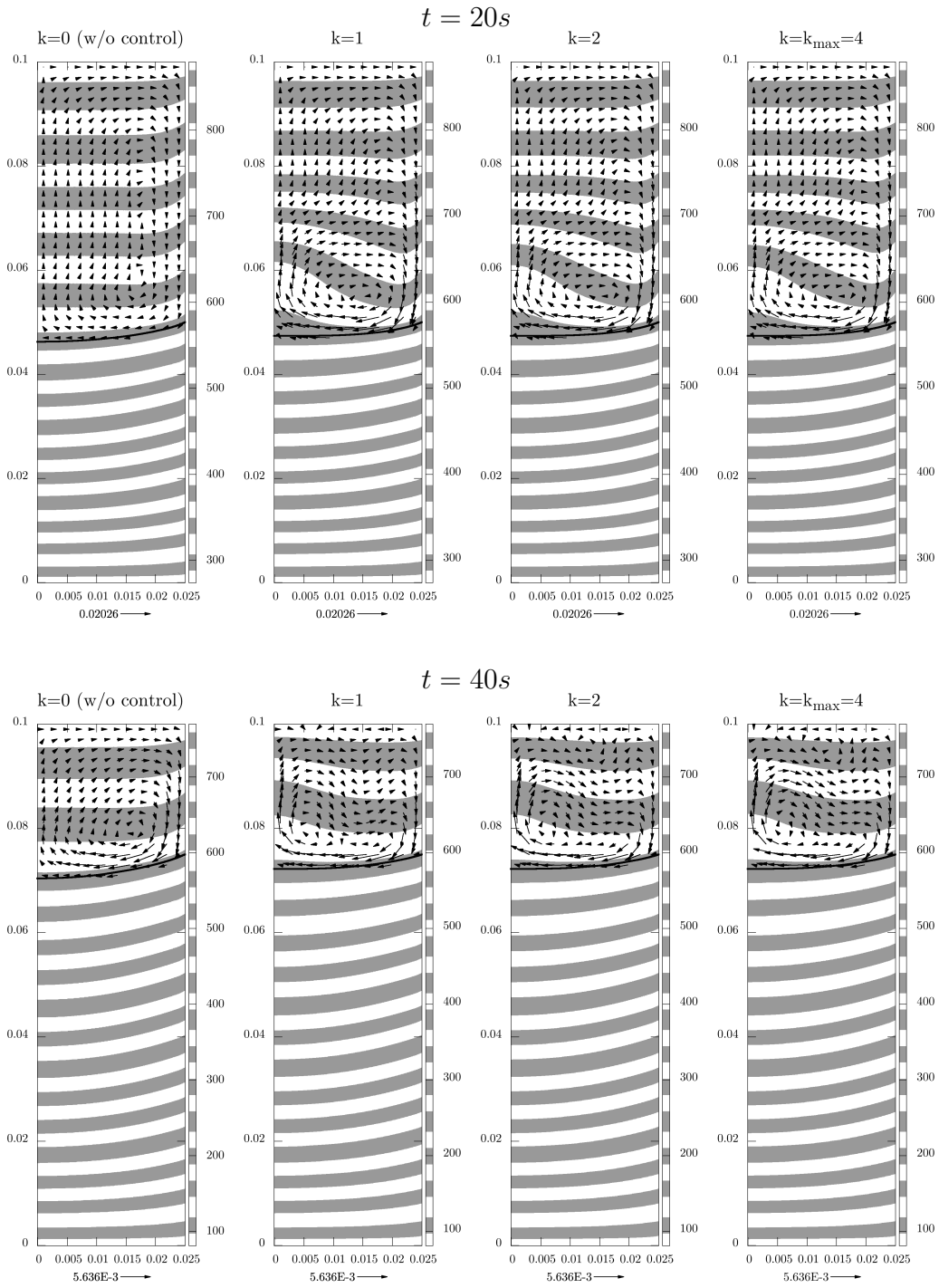

Figure 10: The temperature u (white and grey stripes), velocity (arrows) and free boundary (black line) after several gradient iterations k and at two time instances for the problem with Lorentz force control.

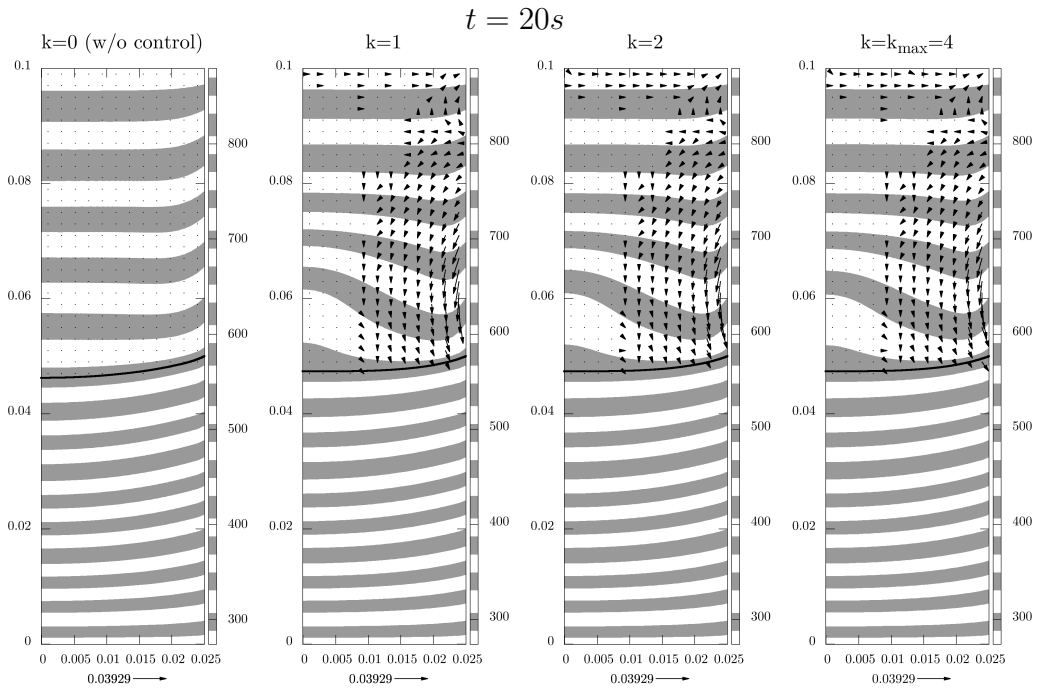

Figure 11: The Lorentz forces (arrows), the temperature u (white and grey stripes) and the free boundary (black line) after several gradient iterations k at $t = 20s$ for the problem with Lorentz force control.

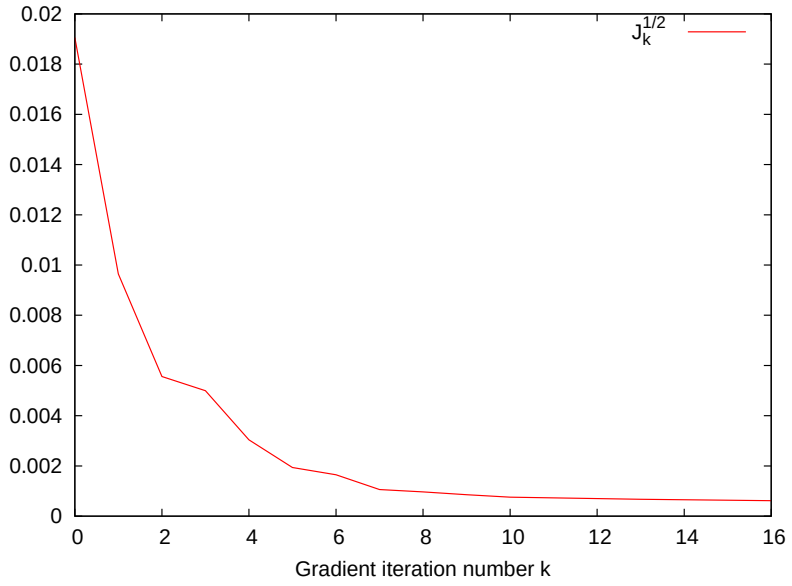

Figure 12: Iteration history of $\sqrt{J}$ for the controlled problem with $\lambda_T = 0.3$ for each gradient step k for the problem with Lorentz force control.

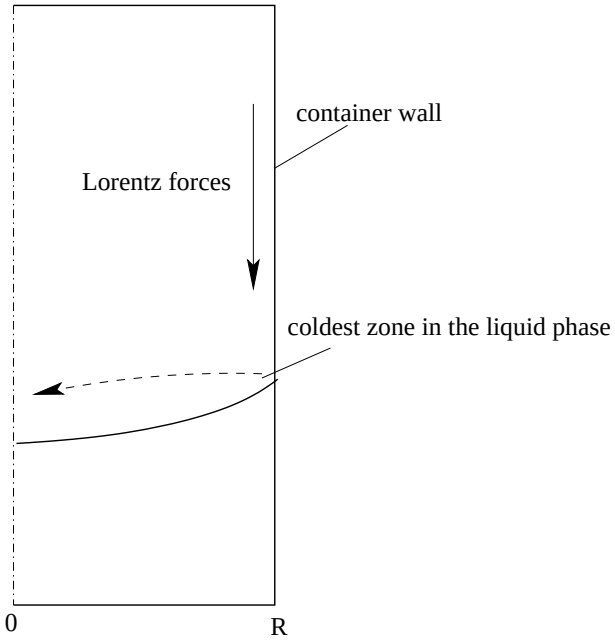

Figure 13: Influence of the flow. In order to achieve a flat free boundary, the cold material must be transported to the center. This is done be Lorentz forces as depicted. Compare also Figures 11 and 10.

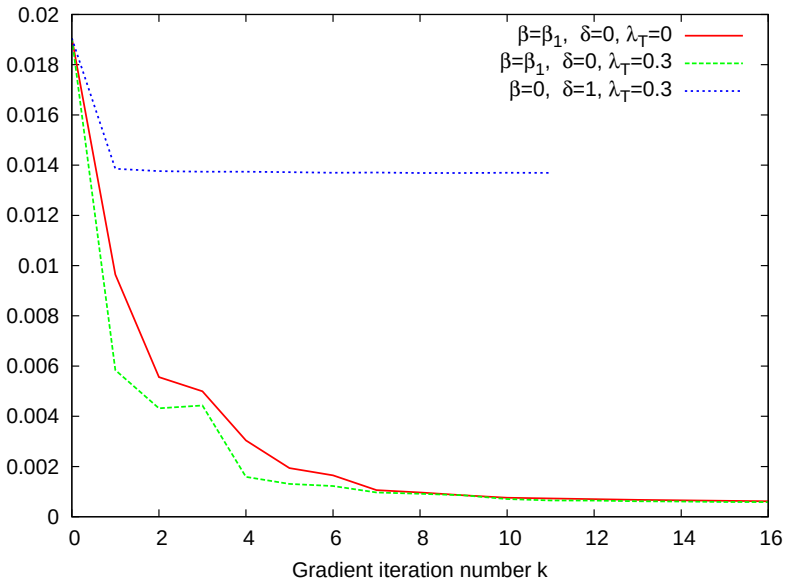

Figure 14: Iteration history of the error of the free boundary $\sqrt{J_0}$ (compare (38)).

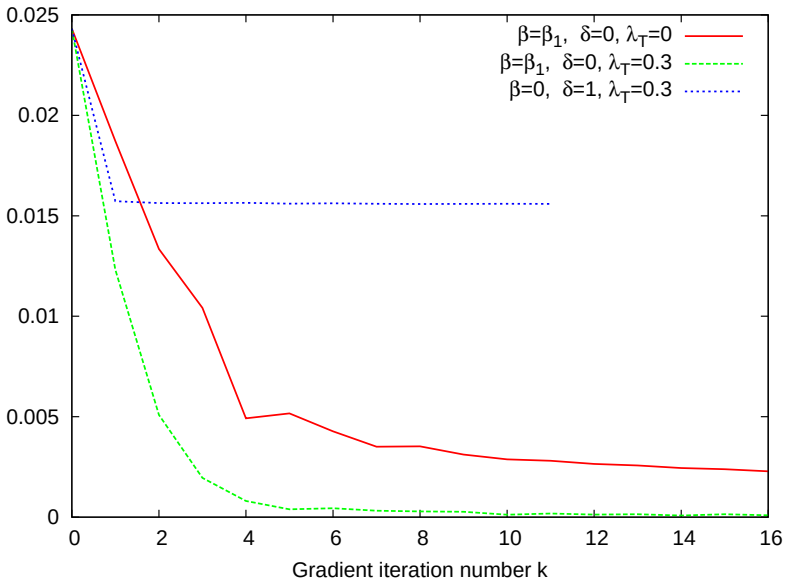

Figure 15: Iteration history of the error of the free boundary $\sqrt{J_T}$ (compare (39)). As expected, for $\lambda_T > 0$ the functional J_T delivers smaller errors than for $\lambda_T = 0$.

4.4 Second test configuration

To demonstrate the scope of control with near-wall Lorentz forces we investigate a melting problem as second test configuration. As above we consider an aluminium melt in a rotation symmetric cylinder with a diameter of $5cm$ and a height of $10cm$. The melting process is optimized over the time period $[0, 62.5s]$. For $\alpha_{s/l}$ we now choose

$$\alpha_s = 50\frac{J}{s \cdot cm^2 \cdot K} \qquad \text{and} \qquad \alpha_l = 200\frac{J}{s \cdot cm^2 \cdot K} \ .$$

The desired free boundary is the moving plane $\overline{f}(t, y) = 0.075m - \frac{1}{1250}\frac{m}{s} \cdot t$ ($t \in [0, T]$, $y \in G$). As initial condition for the temperature we choose

$$u_0(y, h) = u_M + u'_{s/l}(h - 0.075m) \qquad \text{for } y \in G \text{ and } h \in H, \tag{40}$$

where u'_s and u'_l are equal to

$$u'_{s/l} := \frac{L\rho\alpha_{s/l}}{k_{s/l}(\alpha_l - \alpha_s)} \cdot \frac{1}{1500} \cdot \frac{m}{s} \ .$$

For the boundary value u_{b0} we choose

$$u_{b0}\big(t,(y,h)\big) = u_M + u'_{s/l}\big(h - \overline{f}(t,y)\big) \qquad \text{for } t \in [0,T],\ y \in \partial G \text{ and } h \in H. \tag{41}$$

Since we control only using near-wall Lorentz forces, we set

$$\beta = 0\ , \qquad \delta = 1 \qquad \text{and} \qquad \lambda_T = 0.3\ .$$

As above, the spatial mesh contains 100 cells in height and 25 cells in radial direction and we make use of the rotation symmetry.

The numerical results are presented Figure 16 (temperature, velocity and free boundary), 17 (Lorentz forces) and 18 (cost Functional). It can be seen, that the control with Lorentz forces now delivers good results. The free boundary becomes flat by applying Lorentz forces directed upwards at the container wall, see Figure 17. With such a force the hot material is transported to the center with the consequence that the free boundary becomes flat.

4.5 Stopping criterion

Table 3 shows the number of iterations $k_{\max}$ resulting from the stopping criterion (37) with the limit $\varepsilon = 10^{-4}$. The algorithm converges quickly, and needs only 12 iterations; except for the first test configuration with Lorentz force control only, where the shape of free boundary is improved only very slightly. For this case the stopping criterion is already reached after 4 iterations.

Test configuration #	1	1	1	2
β	β_1	β_1	0	0
δ	0	0	1	1
λ_T	0	0.3	0.3	0.3
$k_{\max}$	13	12	4	12

Table 3: The number of iterations $k_{\max}$ resulting from the stopping criterions (37) for all considered cases. As tolerances we set $\varepsilon = 10^{-4}$.

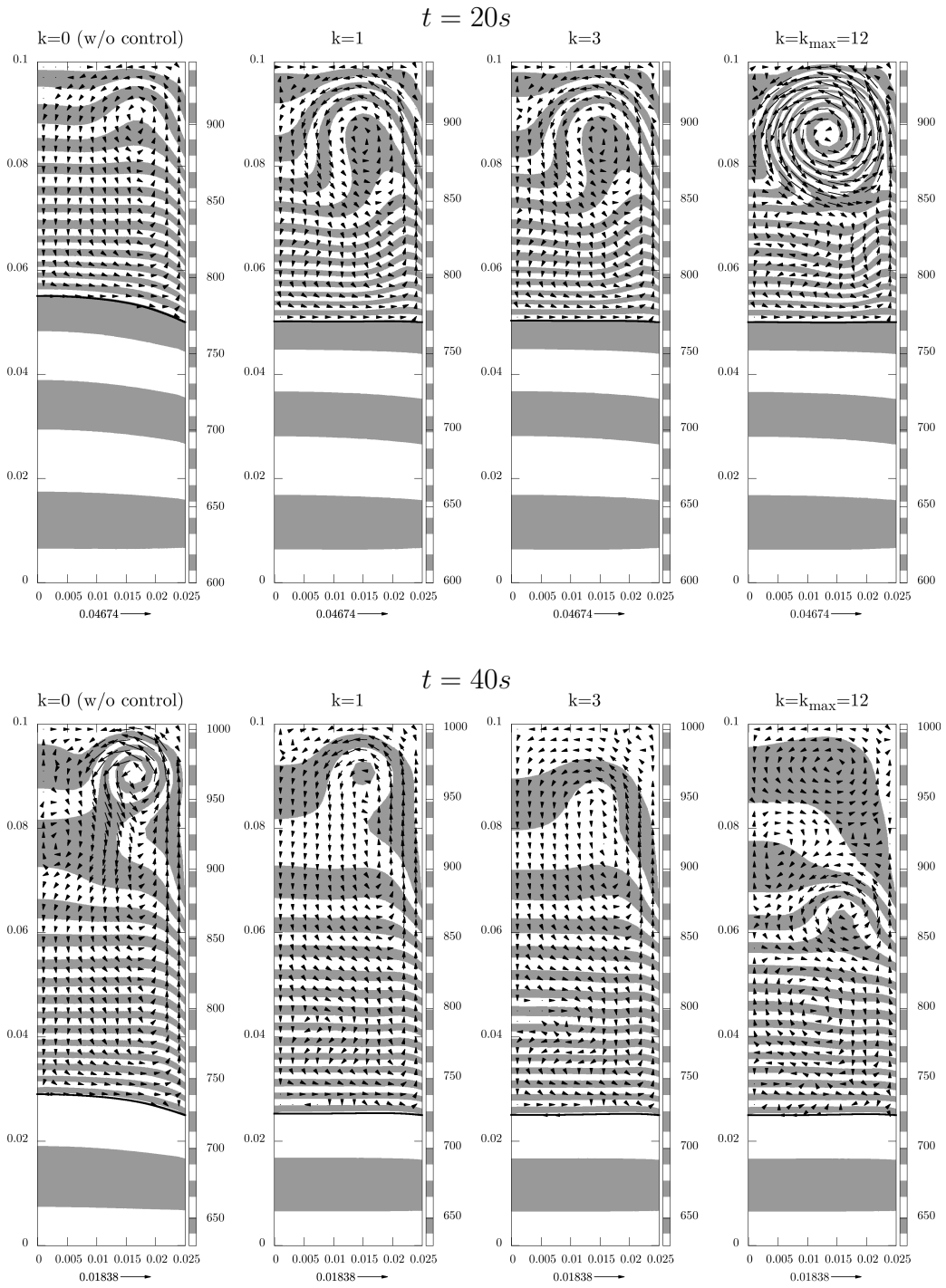

Figure 16: The temperature u (white and grey stripes), velocity (arrows) and free boundary (black line) after several gradient iterations k and two time instances for the melting problem with Lorentz force control.

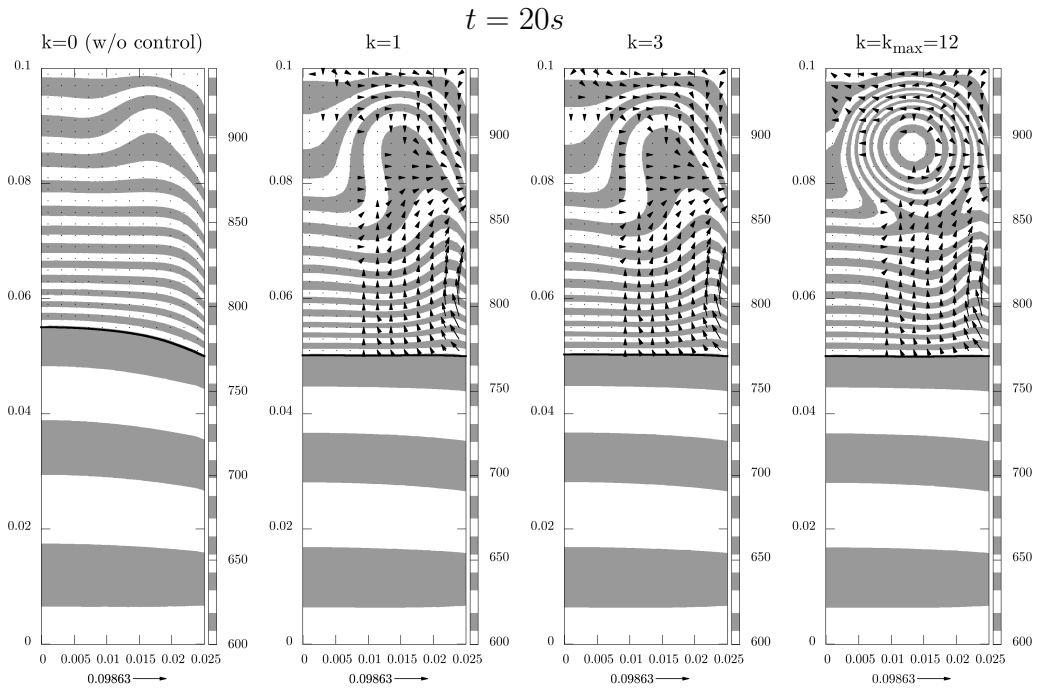

Figure 17: The Lorentz forces (arrows), the temperature u (white and grey stripes) and the free boundary (black line) after several gradient iterations k at $t = 20s$ for the melting problem with Lorentz force control.

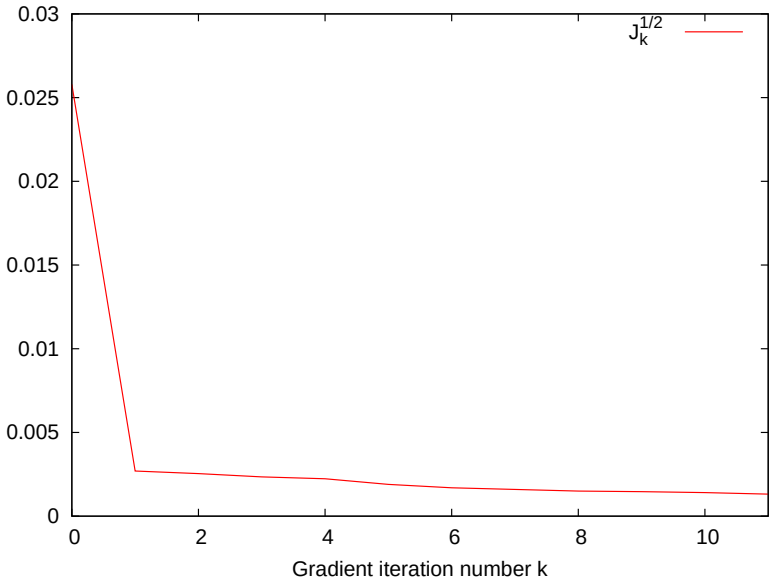

Figure 18: Iteration history of $\sqrt{J}$ for the controlled problem with $\lambda_T = 0.3$ for each gradient step k for the melting problem with Lorentz force control.

Conclusion

We present a control algorithm for the solidification process of a two phase Stefan problem considering flow using a sharp interface model. The control goal consists of tracking a prescribed evolution of the free boundary.

Our optimization approach ensures that the physical laws constituted by our mathematical model hold at every stage of the optimization process. This is accomplished by regarding the interface itself as the optimization variable. We present several numerical examples which demonstrate the scope of our method. It is one result of this work, that the tracking of the interface works very well with container wall temperature control. However with near-wall Lorentz force control only a slight improvement of the shape of the free boundary was possible for the considered solidification problem. On the other hand for the investigated melting problem Lorentz force control also works very well.

References

[1] OpenFOAM: The Open Source CFD Toolbox. http://www.opencfd.co.uk/openfoam/.

[2] T.W. Berger, J. Kim, C. Lee, and J. Lim. Turbulent boundary layer control utilising lth Lorentz force. *Physics of Fluids*, 12(3):631–649, 2000.

[3] M. Hinze and S. Ziegenbalg. Optimal control of the free boundary in a two-phase stefan problem. *Preprint SFB609-2-2005, accepted for publication in JCP*, TU-Dresden, 2005. http://www.math.uni-hamburg.de/home/hinze/Psfiles/sfb609_02-2005_Hinze_Ziegenbalg.pdf.

[4] R.I. Issa. Solution of the implicitly discretised fluid flow equations by operator-splitting. *J. Comput. Phys.*, 62(1):40–65, 1986.

[5] R.I. Issa. An improved PISO algorithm for the computation if buoyancy-driven flows. *Numerical Heat Transfer*, 40:473–493, 2001.

[6] H. Jasak. *Error Analisys and Estimation for the Finite Volume Metod with Applications to Fluid Flows*. PhD thesis, Imperial College of Science, Department of Mechanical Engineering, 1996.

[7] S. Kang and N. Zabaras. Control of the freezing interface motion in two-dimensional solidification processes using the adjoint method. *International Journal for Numerical Methods in Engineering*, 38:63–80, 1995.

[8] T. Weier. *Elektromagnetische Strömungskontrolle mit wandparallelen Lorentzkräften in schwach leitfähigen Fluiden.* PhD thesis, Technische Universität Dresden, Fakultät Maschienenwesen, 2005.

[9] Z. Yang. *The adjoint method for the inverse design of solidification processes with convection.* PhD thesis, Cornell University, 1997.

[10] N. Zabaras and T. Hung Nguyen. Control of the freezing interface morphology in solidification processes in the presence of natural convection. *International Journal for Numerical Methods in Engineering*, 38:1555–1578, 1995.